



STUDY THE EFFECT OF ZIRCONIUM, NICKEL AND HEAT-TREATMENTS ON THE MICROSTRUCTURE AND MECHANICAL PROPERTIES OF COLD-ROLLED AA6111 ALLOY

Saba Jameel Hassan¹, Basem Al-Zubaidy² and Saad Hameed Al-Shafaie³

¹ Department of Metallurgical Engineering, Materials Engineering College, Babylon, University, Babil, Iraq, Email: sabajmeel1228@gmail.com.

² Department of Metallurgical Engineering, Materials Engineering College, Babylon, University, Babil, Iraq, Email: mat.basem.mahsn@uobabylon.edu.iq.

³ Department of Metallurgical Engineering, Materials Engineering College, Babylon, University, Babil, Iraq, Email: mat.saad.hameed@uobabylon.edu.iq.

<https://doi.org/10.30572/2018/KJE/160110>

ABSTRACT

The cold rolling effect on the microstructure and mechanical properties of recycled AA6111 alloy with Zr or/and Ni were investigated. All alloys were produced by the stir-casting method. homogenization heat treatment (500 °C for 6 hours) was performed on AA6111 alloy only. The alloys were solutionized (at 540 °C for 30 minute) and artificially aged (at 180 °C for 10 hours). The optical micrograph, scanning-electron microscope (SEM) and X-ray Diffraction (XRD) studies for all samples. The microstructure analysis displayed different fine intermetallic phases distributed in large amounts in alloys containing Zr or/and nickel compared to AA6111 alloy. The combined alloying elements' addition effect with the cold rolling effect and artificial aging led to great improvements in the mechanical properties, where the hardness and tensile properties of all alloys increased. The AA6111+0.41wt%Ni alloy showed the highest hardness value, as it increased to 161 HV after artificial aging, while the AA6111+0.54wt%Zr alloy showed the highest YS and UTS, which increased to 252 MPa and 342 MPa, respectively.

KEYWORDS

AA6111 aluminum alloy; Al-Mg-Si-Zr-Ni alloys; Cold rolling; Artificial aging; Tensile properties.



1. INTRODUCTION

Presently, AA5xxx or AA6xxx make up the bulk of automotive aluminum sheets that are made, with a tendency toward increasing quantities of AA6xxx because of its greater adaptability (Djukanovic, 2019; Akkar et al., 2023; Raji et al., 2020). Super ductility, corrosion resistance, good formability, medium strength, and manufacturability are just a few of the properties that make AA6111 alloy, one of the greatest significant aluminum alloys from the 6xxx series, the most promising candidate for body panel of automotive manufacturing (Sarkar et al., 2004; Zhang et al., 2013). Grain structure is significant microstructural characteristics of Al automobile alloys as it influences a wide range of the material's properties. Since AA6111 can be riveted in the T6 temper depending on the application, managing the grain structure is crucial when attempting to manage formability. (Mukhopadhyay, 2012) showed that the fine grain structure confirms strengthening by work hardening and grain refinement. One of the methods used to refine or control grain structure is the addition of multiple ingredients, which is a current hotspot of research, where addition of alloying elements to AA6111 alloys in various smaller amounts, e.g. when manganese or chromium is added, the phase that forms is α -Al₁₂(Mn, Fe, Cr)₃Si which can appear as both constituent and dispersoid phases (Mondolfo, 1976). As a result, the size and distribution of the dispersoid particles created during homogenization are adjusted to regulate the grain structure. High-temperature precipitates known as dispersoids are produced during carefully planned homogenization processes (Hatch, 1984). During solution heat treatment, dispersoids function as grain-pinning particles, preventing the formation and growth of new grains during recrystallization. Increasing the strength of the AA6xxx alloys involves many procedures, e.g. the creep behavior of an alloy called AA6111 that has been reinforced by Er, Zr microalloying was studied by (Qian et al., 2023). The microstructure development and high-temperature performance of AA6111 alloy enhanced by Sc, Zr co-microalloying were examined by (Chen et al., 2023). In addition to thermodynamic studies, (Shurkin et al., 2023) investigated the phase composition and microstructure of high-strength AA6xxx aluminum alloys with 0.1, 0.2, and 0.3 weight percent Ni addition. (Babaniaris et al., 2020) developed and evaluated two heat treatment techniques specifically designed to maximize the use of Zr and Sc in an Al-Mg-Si model alloy. A study by (Mikhaylovskaya et al., 2021) examined the effects of eutectic-producing Ni and Fe and dispersoid-producing Sc and Zr alloying elements on the microstructure improvement, super plastic behavior, and tensile parameters for the Al-1.2%Mg-0.7%Si-1.0%Cu alloy at ambient temperature. (Xiao et al., 2017) examined the effects on precipitation and the age-hardening behavior of Al-Mg-Si-xCu (x=0.5, 1.0, 2.5, and 4.5, in weight percentage) alloys when the Cu content was changed.

(Zhang et al.,2017) investigated the mechanical properties, texture, and microstructure evolution of an AA6111 Al-alloy during hot rolling and cold rolling deformation. Cold work's impact on AA6111's precipitation kinetics was assessed by (Quainoo et al., 2004). To examine the differences between traditional symmetric and asymmetric rolling in terms of regulating shear texturing, grain refinement, tensile and plastic-strain ratio mechanical characteristics, (Kang et al., 2005) employed commercial AA6111-alloy sheets.

Due to the increasing development in modern science and technology, the environment in which aluminum components are used has become increasingly harsh, in addition to the urgent need for higher performance of these components. This study aims to enhance the hardness , the yield strength and the ultimate tensile strength of the AA6111 alloys while maintaining good formability by adding Zirconium and/or Nickel and studying the combined effect of adding these elements with cold rolling forming on the strength of these alloys through their kinetics effect of precipitation hardening and obtaining a combination of the composite best requisite properties.

2. EXPERIMENTAL PART

The base alloy utilized in this study was the sheet of the AA6111-T4 with a chemical composition scheduled in Table 1. This alloy has an average Vickers micro-hardness of 89 HV. The added powders of zirconium and nickel were supplied from Changsha Xinkang Advanced Materials Co, Ltd and had an average particle size of 20-30 (μm) and a purity of 99.9 %.

Four experimental alloys (in Table 1) were prepared by stir casting using (Mini MF induction melting furnace). The casting process included melting the AA6111-T4 alloy in a graphite crucible and maintaining it at a temperature of 720 °C. The molten slurry was stirred at a speed of (200 rpm) with a four-blade stirrer for 5 minute under a shield of argon gas. Powders covered with aluminum foil were added to the melt according to their weight percentage. The melted metal was poured onto a heated metallic mold. The resulting cast with dimensions of 200mm in Length, 25mm in width, and 7.5mm in thickness were then exposed to homogenizing heat treatment at 500 °C for 6hours in SRJX-5-13 Model Box-Resistance Furnace and surface milling by 3 mm of the sample thickness. Then, the samples were rolled at room temperature at a constant speed rate of 32 rpm with a roller diameter of 27cm . The rolling process is repeated for 14 passes, and with each pass reduction of 2.5% in thickness was obtained, until reaching a reduction rate of 35% of the original thickness. After completing the rolling process, the rolled sheets were solution heat treated at 540°C for 30 minute and quenched in ice for 5 minutes. This treatment was followed by artificial aging at 180 °C for 10 hours according to (Quainoo

et al., 2011). The AA6111, AA6111+0.54%Wt%Zr, AA6111+0.41wt%Ni, AA6111+0.43wt%Zr +0.85wt%Ni alloys then underwent Chemical composition according to ASTM-E1251-17a, Microstructure observation, SEM, XRD, Hardness, and Tensile tests.

Table 1. The nominal prepared alloys Chemical composition

Alloy	Si%	Mg%	Cu%	Fe%	Zr%	Ni%	Al%
AA6111	0.685	0.722	0.969	0.43	0.007	0.004	Bal.
AA6111+Zr	0.697	0.678	0.982	0.35	0.54	0.002	Bal.
AA6111+Ni	0.678	0.707	0.914	0.419	0.002	0.41	Bal.
AA6111+Zr+Ni	0.648	0.683	0.907	0.416	0.43	0.85	Bal.

For metallography experiments, specimens in different conditions were prepared following the standard metallography preparation procedure (i.e. several grinding and polishing steps). Followed by etching in 95 ml of water, 2.5 ml of nitric acid, 1.0 ml of hydrochloric acid, and 1.5 ml of hydrofluoric acid according to ASTM E407-07 (A. S. T. M. 2012). Optical microscope model YJEYE01 photographed the microstructure of the surface. Furthermore, the Vickers microhardness test was conducted according to ASTM (E384) (Hetzner, 2003) with a load of 200g and loading time of 10 seconds for all the cast, homogenized, rolled, quenched, and aged samples. After completing all the processing procedures for the prepared alloys (homogenization treatment, rolling, solution treatment, quenching, and artificial aging), Three tensile samples were cut in a direction parallel to the rolling direction (DR) by using Wire Electrical Discharge Machining (WEDM) according to ASTM E08-04. All samples were ground with SiC grinding papers to 1500 grades and then polished to remove any surface defects. The test was performed with a strain rate of 1 mm/min according to (Al-Zubaidy, 2017). The SEM was utilized to show the microstructure with high accuracy to characterize the surface shape and identify the difference among the aged specimens. Also, XRD analysis was used to determine the stoichiometry of secondary phases present in the matrix of all alloys and their relative proportions. The particle size was also measured using Image-J and Origin-Pro 2024b programs based on the SEM images.

3. RESULTS

3.1. Microstructure

Al-Mg-Si alloy SEM images and EDS analysis demonstrations are in Fig. 2. As shown in Fig.2(a), the microstructure of as-cast AA6111 alloy consists of α -Al dendrites (light phase) with irregular orientations and inter-dendritic regions of the eutectic phase (dark area) formed and distributed between grain boundary and dendrite cell boundary. However, the average grain

size was measured at 62 μm for casted AA6111 alloy. After homogenization heat treatment, some intermetallic compounds distributed between grain and dendrite cell boundary began dissolving in the matrix gradually with increasing temperature and soaking time as shown in Fig. 2(b), the alloy structure after homogenization treatment possesses grains with an average size of 51 μm .

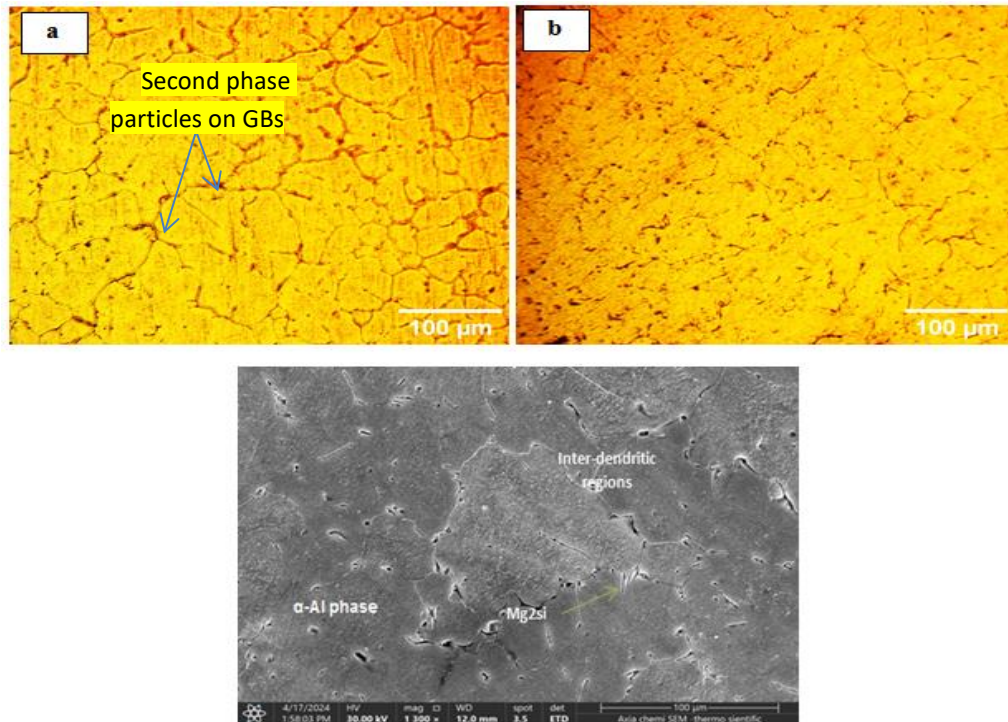


Fig.1. Optical micrographs and SEM of AA6111 alloy (a) as cast; (b) homogenized .

The SEM data from Fig.1 for the homogenized AA6111 alloy shows the α -Al dendrites and interdendritic regions of the eutectic phase formed between α -Al dendrites. Also shows the Mg₂Si phase, which seems in the black Chinese script particle form; this is the same as stated in (Al-Helal et al., 2020).

The morphology of grain transformed progressively from a near-equiaxed shape and homogeneous microstructure to an elongated shape with nonhomogeneous microstructure during the rolling process as shown in Fig. 2(a). Also, the cold rolling process reduced the porosity. The effect of the solution heat treatment on the grain structure of this alloy is clear, which led to a recrystallized microstructure, thus the AA6111 possesses a refined grain size and morphology as shown in Fig. 2(b). Performing the aging treatment after solution treatment and quenching led to a reduction in the grain size of the alloy with a range of 22 μm and also showed a more homogeneous structure as shown in Fig. 2(c).

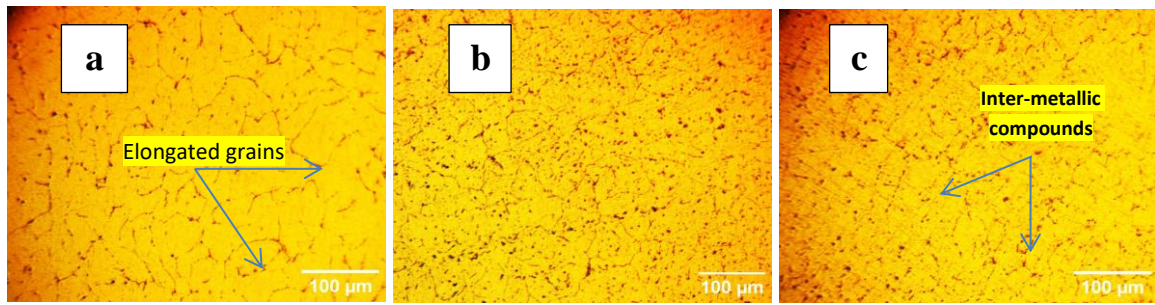


Fig. 2. Optical image of AA6111 alloy (a) after rolling; (b) after solution heat treatment and quenching; (c) after ageing at 180°C for 10hrs .

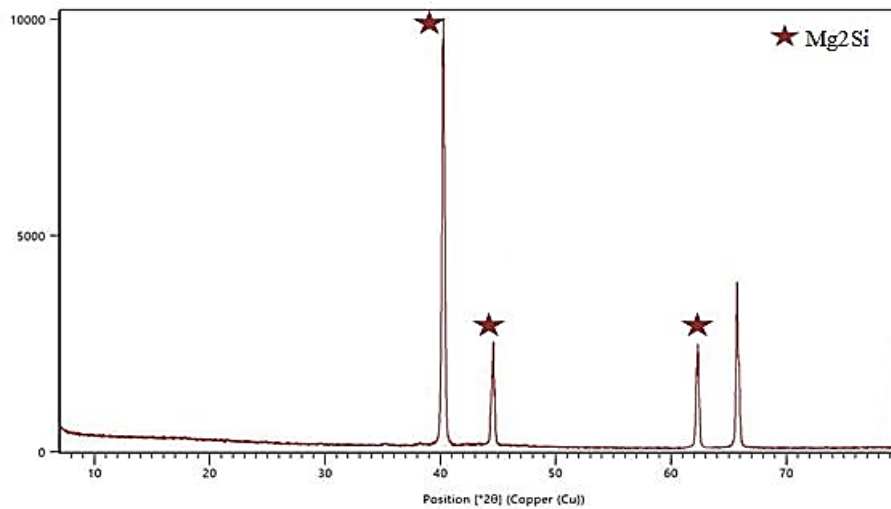


Fig.3. XRD analysis of the AA6111 alloy after artificial ageing at 180°C for 10hrs.

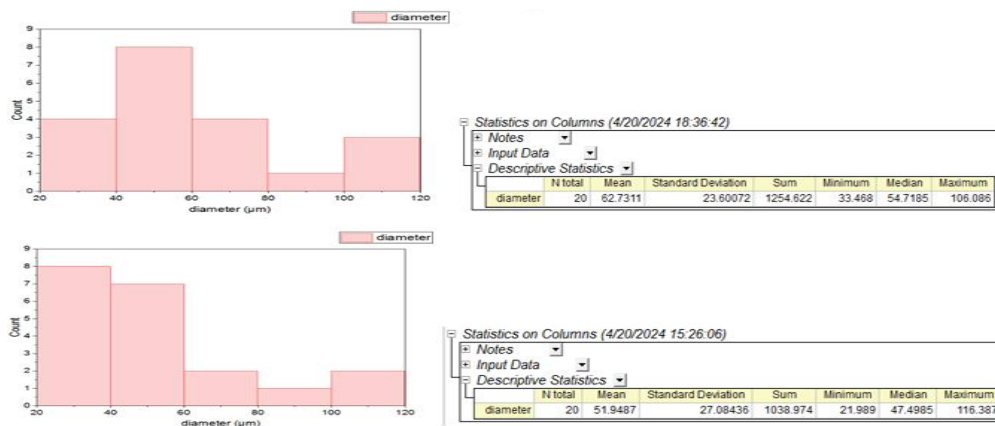


Fig.4. Grain size plots from Image J and Origin Pro analysis programs.

The structure of the as-cast A6111 alloy has a substantial amount of constituents, as seen in Fig. 1(a), which exist in irregular forms and cause the production of a dendritic network structure. Following conventional casting techniques, Al-Mg-Si alloys consolidate, and throughout a broad range of cooling rates, the form of these dendrites does not significantly change (Zeren, 2005). In Fig. 5, we notice that the number of constituents of this alloy rises with the zirconium addition, and this led to noticeable refining in the as-cast microstructure

where the average grain size of casted AA6111+0.54wt%Zr was 35 μ m. Zirconium addition might consequence of this alloy grain refinement because of fine Al₃Zr particles, as shown in Fig.5 in the SEM image, which act as nucleation sites during the recrystallization process (Dang et al., 2009). Larger, longer Al₃Zr phase particles were discovered inside or on the edges of the grains (Jiao et al., 2023).

In Fig. 7(a), it is noted that the grain shape after the cold rolling process is almost equiaxed and has little elongation compared to the casted or homogenized AA6111 alloy, as a result of the presence of intermetallic compounds containing zirconium element, which hinder the movement of grain boundaries and prevent their elongation when applying a pressure force on them by the rollers. After SHT and aging treatment of the rolled AA6111+0.54wt%Zr alloy as shown in Fig. 7 (b,c), the grains that deformed are changed by an undeformed and unstressed new set grains. Consequently, the recrystallization process reduces the strength of the alloy's hardness. The recrystallization process in this alloy slows down significantly due to the precipitate of fine intermetallic compound or particles containing zirconium element due to Zener pinning, therefore the grain size decreased from 62 μ m in the as-cast AA6111 alloy to 16 μ m for the AA6111+0.54wt%Zr alloy. The XRD patterns for AA6111+0.54%Wt%Zr alloy shown in Fig.6 which show peaks for the Al₃Zr and Mg₂Si phases.

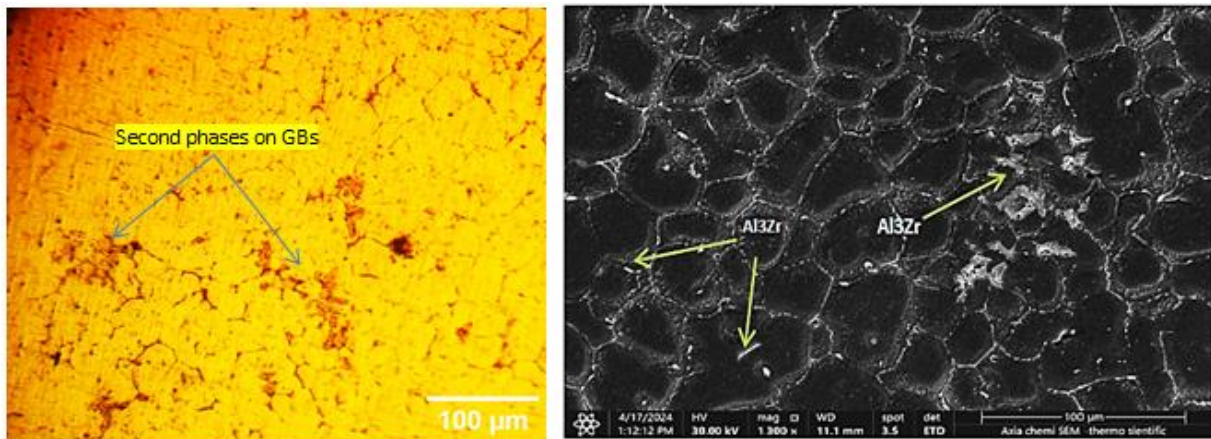


Fig. 5: Optical image and SEM of casted AA6111+0.54wt%Zr alloy.

As presented in Fig. 1(a, b) and Fig. 5, the grain size of the casted and homogenized AA6111 alloy differs significantly from AA6111+0.41wt%Ni alloy, where the average grain size of the casted AA6111+0.41wt%Ni alloy was 31 μ m. As a result, the nickel addition to the AA6111 alloy led to an important and noticeable improvement in the structure. In the as-cast AA6111 structure, the precipitated phase is different in AA6111+0.41wt%Ni alloy, and it is reflected in the morphological variance, as the phase(Mg₂Si) that precipitated in the as-cast AA6111alloy is in the black Chinese script particles form, while the precipitated phase(Al₃Ni) in AA6111 alloy due to the addition of nickel is a broad network and the shape as like to fishbone (Zuo et

al., 2020) as shown in Fig. 8 in the SEM image. The addition of trace elements such as nickel produces alloys with properties that differ from alloys without the trace elements addition. From XRD results, the precipitate of the Al_3Ni phase is observed mainly in addition to other intermetallic compounds such as $\text{Al}_{1.9}\text{CuMg}_{4.1}\text{Si}_{3.3}$ and $\text{Al}_9\text{Fe}_{0.8}\text{Mn}_{2.16}\text{Si}$ as shown in Fig. 9.

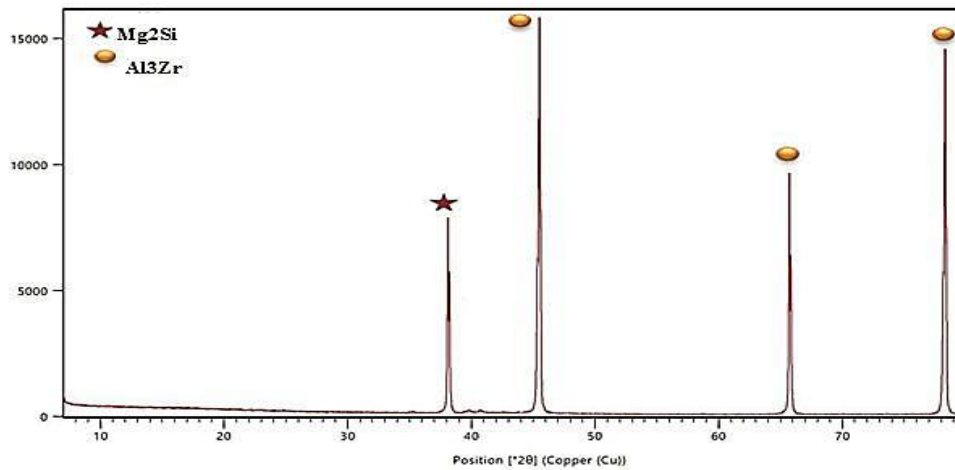


Fig. 6: XRD analysis of the AA6111+0.54%Wt%Zr alloy after artificial ageing at 180°C for 10hrs.

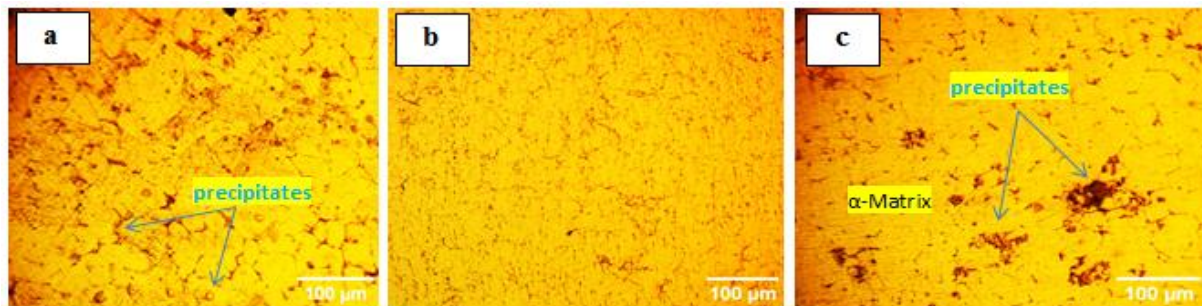


Fig. 7. Optical images of AA6111+0.54wt%Zr alloy (a) after rolling; (b) after solution heat treatment and quenching; (c) after aging at 180°C for 10hrs.

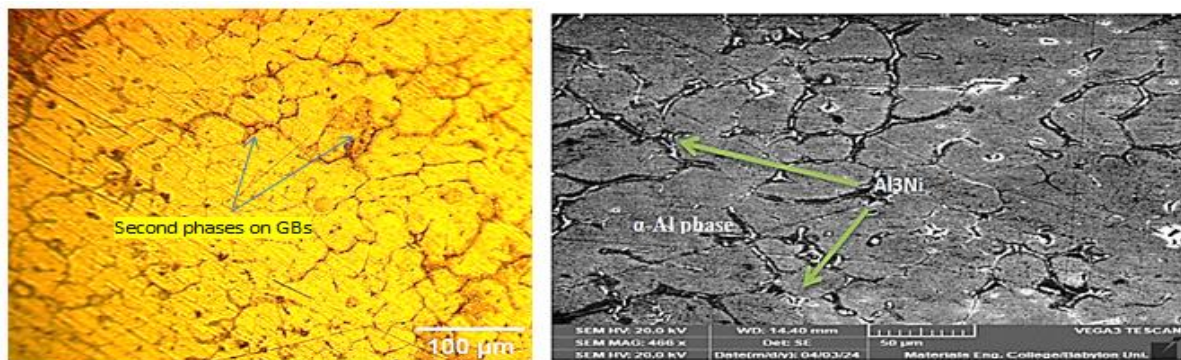


Fig. 8. Optical micrographs and SEM of casted AA6111+0.41wt%Ni alloy.

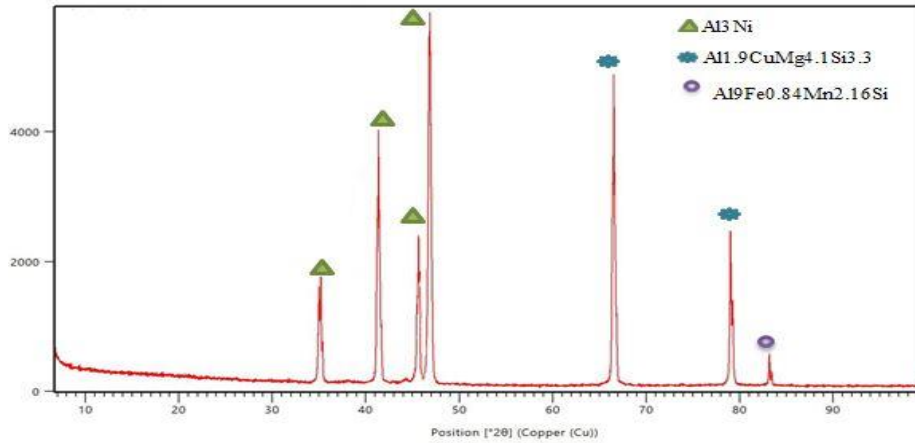


Fig.9: XRD analysis of the AA6111+0.41wt%Ni alloy after artificial ageing at 180°C for 10hrs.

During the rolling process, pinning the grain borders and impeding grain development are the fine Ni-rich phase particles. The volume percentage and size of the tiny particles determine the pinning force, so the grain size in AA6111+0.41wt%Ni alloy is much smaller (average grain size 21 μ m) compared to the grain size of the casted and homogenized AA6111 alloy after 14 passes as shown in Fig. 10(a), which enhances the mechanical properties of AA6111+0.41wt%Ni alloy.

The effect of both solution treatment at 540 °C for 30 minutes and artificial aging treatment at 180 °C for 10 hours is shown in Fig. 10(b,c).

These micrographs show that the face-centered cubic solid solution α (Al) is the dominant phase in the microstructure of the alloy with the presence of intermetallic compounds in the structure, where these intermetallic compounds are distributed uniformly. It was noted that AA6111+0.41wt%Ni alloy contains more intermetallic compounds such as Al₃Ni and Mg₂Si than the base alloy as a result, the average grain size of AA6111+0.41wt%Ni alloy after artificial aging was 14 μ m, which enhances better mechanical properties.

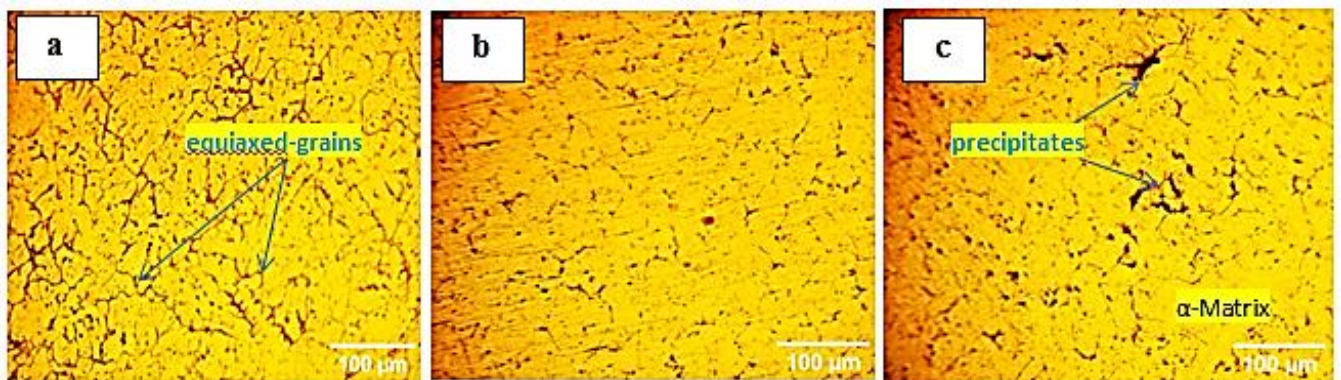


Fig. 10. Optical micrographs of AA6111+0.41wt%Ni alloy (a) after rolling; (b) after solution heat treatment and quenching; (c) after aging at 180°C for 10hrs.

Fig. 11, show optical micrographs and SEM of the combined influence of adding both zirconium and nickel to the AA6111 alloy in terms of the effect on the grain size and shape, the number of intermetallic compounds formed compared to the AA6111 alloy, impeding grain growth and stabilizing grain boundaries, the recrystallization process after solution treatment, and what phases are precipitated after Artificial aging treatment and its effect on the mechanical properties of this alloy. The XRD results in Fig. 12 confirm the appearance of the intermetallic compounds Al_3Zr and Al_3Ni in the AA6111+0.43wt%Zr+0.85wt%Ni alloy.

The addition of both zirconium and nickel makes the grains finer compared to the other alloys due to the fine Al_3Zr and Al_3Ni particles, where the average grain size of the casted AA6111+0.43wt%Zr +0.85wt%Ni alloy was $22\mu m$. These fine particles have an effective role in stabilizing the grain boundaries and hindering grain growth during the cold rolling process, as it is noted that the shape of the grains is approximately equal, and the average size of the particles after cold rolling was $16\mu m$ as noted in Fig. 13(a). These fine particles also work as nucleation sites during the recrystallization process. The amount of these fine particles or intermetallic compounds precipitate after casting or aging was greater than the casted and homogenized AA6111 alloy, so the average grain size of the AA6111+0.43wt%Zr +0.85wt%Ni after the precipitation process was $11.9\mu m$, thus obtaining better mechanical properties.

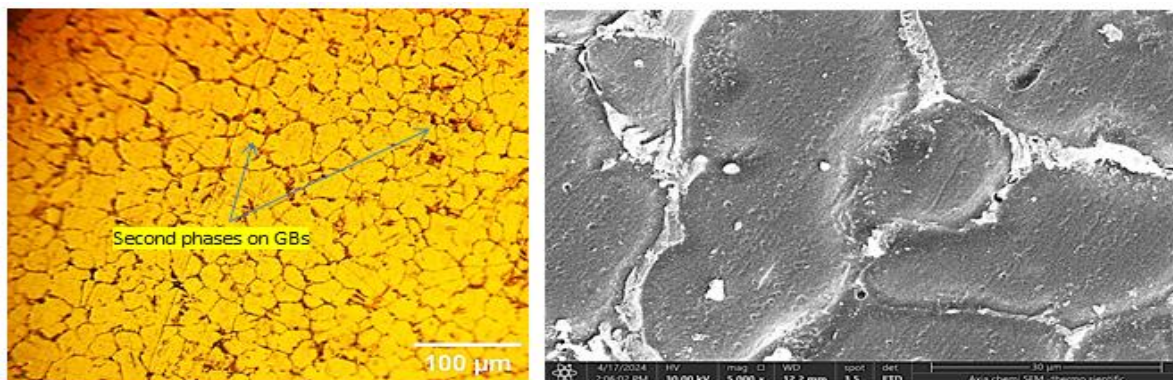


Fig. 11. Optical micrographs and SEM of casted AA6111+0.43wt%Zr +0.85wt%Ni alloy.

The addition of both zirconium and nickel makes the grains finer compared to the other alloys due to the fine Al_3Zr and Al_3Ni particles, where the average grain size of the casted AA6111+0.43wt%Zr +0.85wt%Ni alloy was $22\mu m$. These fine particles have an effective role in stabilizing the grain boundaries and hindering grain growth during the cold rolling process, as it is noted that the shape of the grains is approximately equal, and the average size of the particles after cold rolling was $16\mu m$ as shown in Fig. 13(a). These fine particles also work as nucleation sites during the recrystallization process. The amount of these fine particles or intermetallic compounds precipitate after casting or aging was greater than the casted and

homogenized AA6111 alloy, so the average grain size of the AA6111+0.43wt%Zr +0.85wt%Ni after the precipitation process was 11.9 μm , as shown in Fig. 13(c), thus obtaining better mechanical properties.

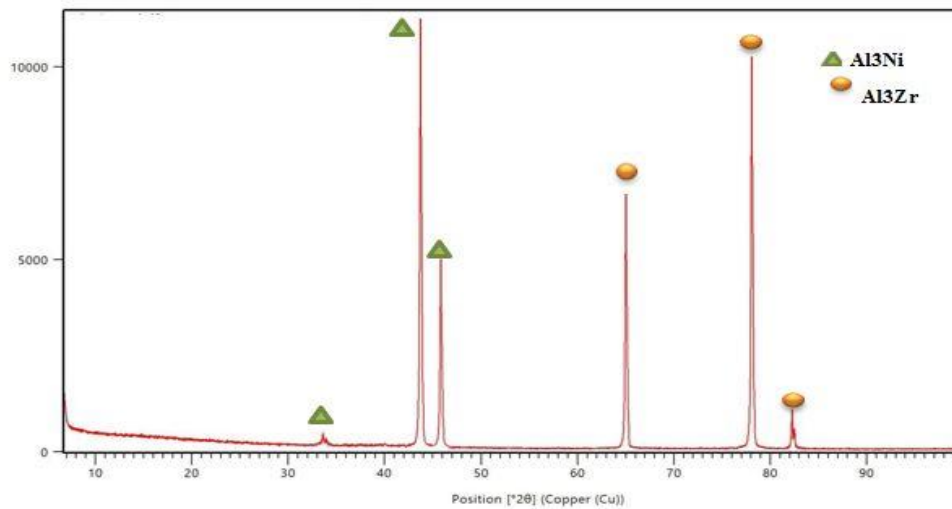


Fig. 12: XRD analysis of the AA6111+0.43wt%Zr+0.85wt%Ni alloy after artificial ageing at 180°C for 10hrs.

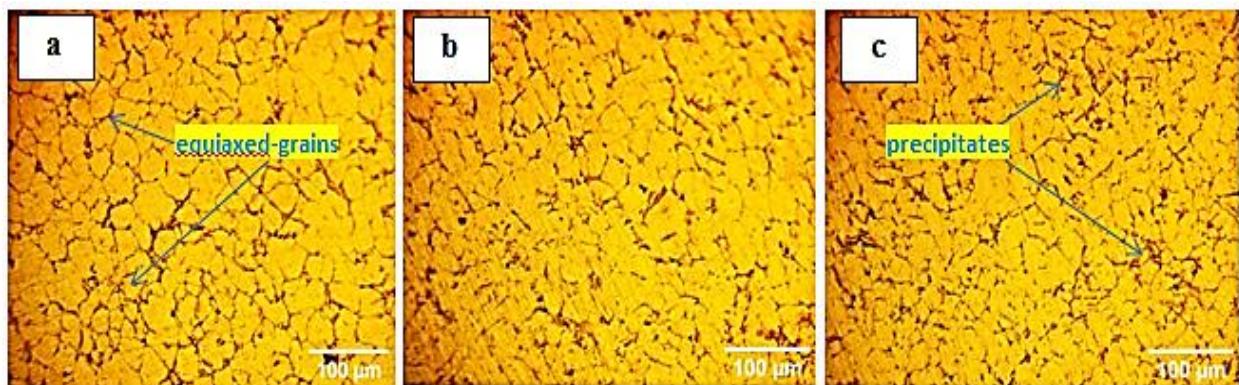


Fig. 13. Optical micrographs of AA6111+0.43wt%Zr +0.85wt%Ni alloy (a) after rolling; (b) after solution heat treatment and quenching; (c) after aging at 180°C for 10hrs.

3.2. Microhardness result

From Fig. 14, it is clear that the AA6111 alloy containing Zr or/and Ni has much higher hardness than the AA6111 alloy in the as-cast state, this is due to the change in the shape of the primary grains from a dendritic structure to a fine, equiaxed structure. The strongest effect on the Vickers hardness was observed at AA6111+0.54wt%Zr alloy. During the Al-alloys casting, a large portion of the alloying elements separate and accumulate in the liquid phase, which leads to a heterogeneous distribution of these elements in the microstructure. Similarly, if phases created during casting are found inside or near grain boundaries, they may also cause segregation. Therefore, this heterogeneous distribution of the alloying elements and fine particles is removed by homogenization treatment, which ensures the decomposition of these

phases and redistributed homogeneously within the structure, this explains the reason for the decrease in the hardness of AA6111 alloy after the homogenization process to 77 HV. The alloy's hardness values were much higher after cold rolling compared to those in the as-cast form, but the strongest effect of hardness is still for AA6111+0.54wt%Zr alloy. This is because the microstructure of casted and homogenized AA6111 alloy becomes severely deformed when it is deformed at room temperature and because the density of dislocations increases after cold rolling, the metal hardness and strength increase, but is escorted by a ductility decreasing. The addition of zirconium and/or nickel to AA6111 alloy acts as an obstacle to the movement of dislocations, and this means a much greater dislocations density increment in the structure of these alloys compared to the AA6111 alloy. After performing the solution treatment process, the hardness value decreases to 61–68 HV. This is due to the increase in the number of vacancies in the matrix with an equilibrium increase in temperature (Cahn et al., 1996), where the rapid cooling of the alloys after solution treatment (quenching) leads to fixing these vacancies formed at high temperatures in the matrix in place at room temperatures.

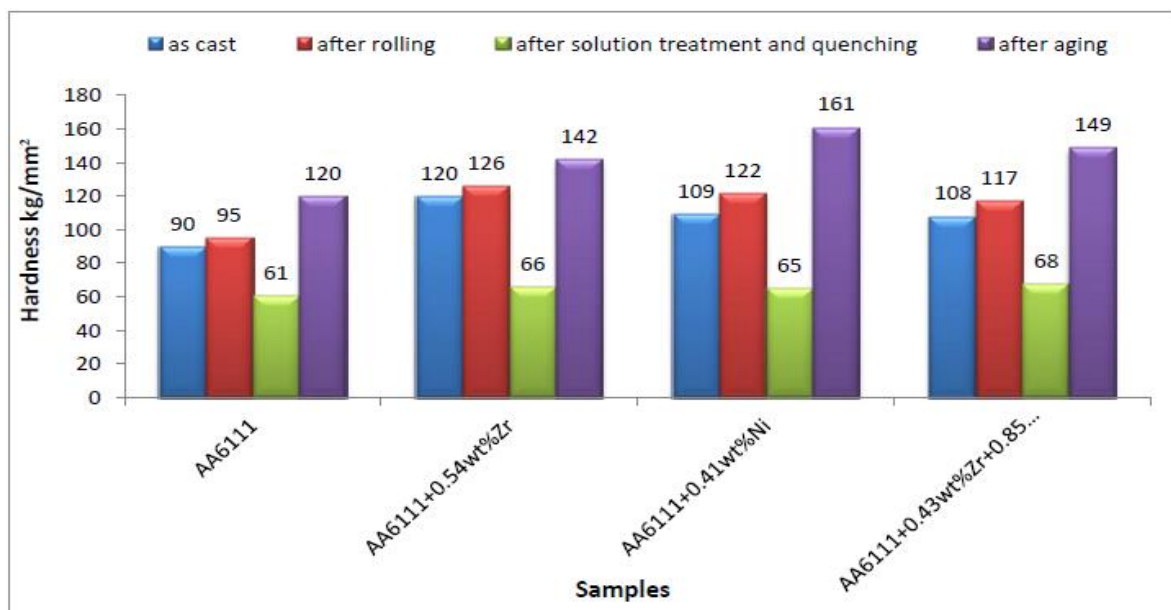


Fig. 14. Average Vickers microhardness for all samples

The highest hardness values were recorded after the artificial aging of all alloys for some reasons:

- The fine intermetallic compounds or particles formed from the casting process act as sites of nucleation through the recrystallization process, and the dislocations also provide sites for precipitation during aging.

- The effect of cold rolling affects the response of precipitation hardening, where the greater the cold rolling reductions, the lower the temperature required to enhance strengthening by precipitation. This is due to a rise in the defect density in the material, thus allowing the spread of alloying elements and the subsequent growth of precipitates (Zhen et al., 1997).

The highest hardness values after artificial aging were observed for AA6111+0.41wt%Ni alloy. This is due to the amount of fine intermetallic compounds or precipitates formed in this alloy after artificial aging.

3.3. Tensile test results

Fig. 15, illustrates the Stress-Strain curves of the rolled and aged alloys in the peak-aged state with the tensile curve of the as-cast AA6111 alloy. Data such as ultimate tensile strength and yield strength were recorded in Table 2.

Table 2. The results of Tensile Tests

Samples	Yield Point (MPa)	Ultimate Tensile Strength (MPa)
As cast AA6111	153	281
AA6111 after ageing	158	290
AA6111+0.54wt%Zr after ageing	252	342
AA6111+0.41wt%Ni after ageing	213	323
AA6111+0.43wt%Zr+0.85wt%Ni after ageing	201	320

These values offer vision into the mechanical behavior of these alloys and their strength after cold rolling and artificial aging. where the standard tensile value for AA6111 alloy is 280 MPa (Totten et al., 2003). The microstructure that are anisotropic where formed through sheet rolling was shown to be responsible for controlling the mechanical features of Al-alloy sheets by (Okayasu et al., 2012). It is commonly known that when Al-alloy sheets are rolled and heated, plastic anisotropy occurs, so adding zirconium and/or nickel improves all alloys' ultimate tensile strength, especially when compared to AA6111 without these elements. It is worth noting that AA6111+0.54wt%Zr alloy, cold rolled at a reduction rate of 35% and artificially aged, has the highest UTS compared to other alloys. This difference in UTS between the alloys containing zirconium or/and nickel and the AA6111 alloy without the addition of these elements is because the increase in the dislocations density leads to dislocation hardening, which is beneficial to improving strength, as well as the presence of precipitates on the grain boundaries, which leads to grain refinement strengthening. it is also useful in enhancing these alloy's strength.

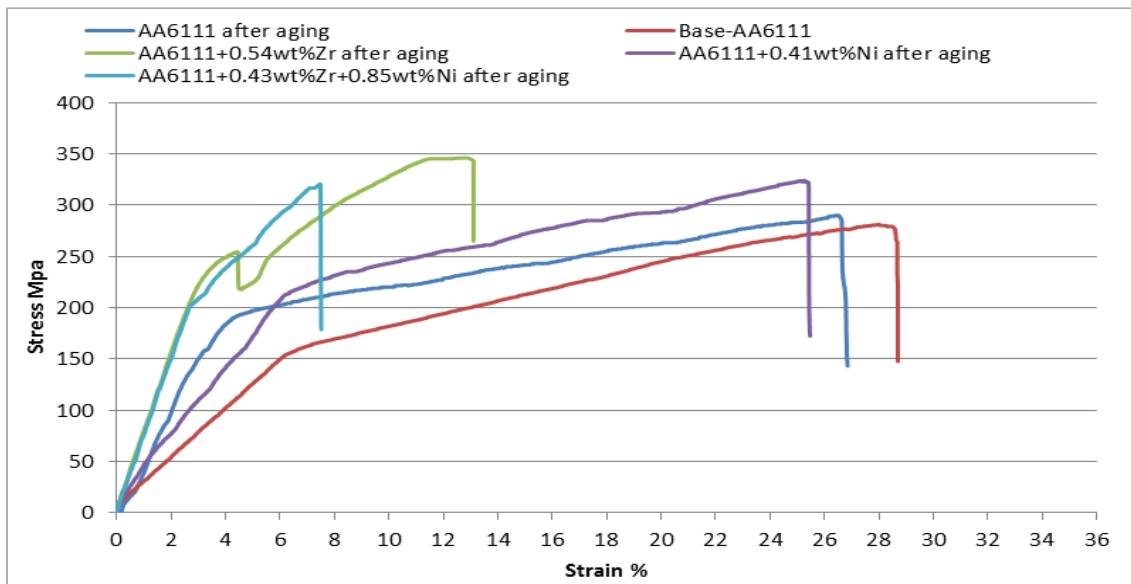


Fig. 15. The Stress-Strain Curve for the prepared alloys under different conditions.

4. CONCLUSION

In this work, the effect of both nickel and zirconium additions on AA6111 alloy was studied, as well as the combined effect of these additions with cold rolling, and artificial aging on the mechanical properties of the resulting alloys. According to the obtained results, the main conclusions may be summed up as follows:

1. The addition of zirconium and/or nickel resulted in a very significant grain refinement.
2. The increase of dislocations as a result of cold rolling, in addition to the role of the added alloying elements in hindering the movement of these dislocations, led to an increase in the hardness of all alloys especially the alloys containing zirconium and/ or nickel after cold rolling, as the highest hardness value was for the AA6111 + 0.54wt%Zr alloy, but The highest hardness value after artificial aging was for AA6111+0.41wt%Ni alloy, due to the number of precipitates or inter-metallic compounds formed in this alloy after artificial aging.
3. The dislocation hardening and grain refinement strengthening led to an enhancement of YS and UTS of all alloys after artificial aging, as the AA6111+0.54wt%Zr alloy showed an important improvement in the yield strength and tensile resistance, where the YS increased to 252 MPa and the UTS to 342 MPa. Also, the UTS of AA6111 alloy thermally homogenized before cold rolling increased from 281 to 290 MPa.

ACKNOWLEDGEMENT

The authors are grateful for the financial support towards the Metallurgical Engineering Department, College of Materials Engineering, Babylon university I wish to express my deepest thanks to the staff of the laboratories for their assistance.

5. REFERENCES

- Akkar, A. Y., and Alali, M. (2023). 'Resistance spot welding of dissimilar metals AISI 1006 low carbon steel and AA6061 aluminum alloy using zing and tin coating'. *Kufa Journal of Engineering*, 14(3), 1-16.
- Al-Helal, K., Patel, J. B., and Fan, Z. (2020) 'Fe-rich intermetallic formation and mechanical properties of recycled AA6111 alloy strips produced by melt conditioning twin roll casting', *Journal of JOM*, 72(11), 3753-3759.
- Al-Zubaidy, B. M. M. (2017) 'Material interactions in novel refill friction stir spot welding approach to join Al-Al and Al-Mg automotive sheets', The University of Manchester (United Kingdom).
- Babaniaris, S., Ramajayam, M., Jiang, L., Langan, T., and Dorin, T.(2020) 'Tailored precipitation route for the effective utilization of Sc and Zr in an Al-Mg-Si alloy', *Materialia*, 10, 100656.
- Cahn, R. W., & Haasen, P. (Eds.). (1996) , *Physical metallurgy* (Vol. 1). Elsevier.
- Chen, G., Kai, X., Tao, R., Cao, R., Qian, W., and Zhao, Y. (2023) 'Microstructure evolution and high-temperature performances of AA6111 alloy strengthened by Sc, Zr co-microalloying', *Materials science and engineering journal, A*, 887, 145788.
- Dang, J. Z., Huang, Y. F., and Cheng, J. (2009) 'Effect of Sc and Zr on microstructures and mechanical properties of as-cast Al-Mg-Si-Mn alloys', *Journal of transactions of nonferrous metals society of china*, 19(3), 540-544.
- Djukanovic, G. (2019) 'Aluminum Alloys in the Automotive Industry: A Handy Guide', *Journal of Aluminum Insider*.
- G. E. Totten and D. S. MacKenzie. (2003) 'Handbook of Aluminum, vol. 1, physical metallurgy and processes, vol. 1', CRC Press.
- Hatch, J. E. (1984) 'Aluminium Properties and Physical Metallurgy', American Society for Metals.
- Hetzner, D. W. (2003) 'Microindentation hardness testing of materials using ASTM E384' *Microscopy and microanalysis journal*, 9(S02), 708-709.
- Jiao, L., Wang, B., Zhao, Y., Wang, K., Li, F., and Li, H. (2023) 'Microstructure and plastic instability of (ZrB₂+ Al₃Zr)/AA6016 composites prepared by melt reaction method', *Journal of materials engineering and performance*, 32(5), 2509-2521.

- Kang, S. B., Min, B. K., Kim, H. W., Wilkinson, D. S., and Kang, J. (2005) 'Effect of asymmetric rolling on the texture and mechanical properties of AA6111-aluminium sheet', *Metallurgical and materials transactions journal A*, 36, 3141-3149.
- Mikhaylovskaya, A. V., Ghayoumabadi, M. E., and Mochugovskiy, A. G.(2021) 'Superplasticity and mechanical properties of Al-Mg-Si alloy doped with eutectic-forming Ni and Fe and dispersoid-forming Sc and Zr elements', *Materials Science and Engineering, A*, 817, 141319.
- Mondolfo, L.F. (1976) 'Aluminium Alloys: Structure and Properties', Butterworths and Co., Ltd., London, 806.
- Mukhopadhyay, P. (2012) 'Alloy designation, processing, and use of AA6XXX series aluminum alloys', *International scholarly research notices*.
- Okayasu, M., Sato, R., Takasu, S., Niikura, A., and Shiraishi, T. (2012) 'Mechanical properties of AlSiCu alloys produced by the twin rolled continuous casting process', *Journal of materials science and engineering, A*,534, 614-623
- Qian, W., Kai, X., Tao, R., Gao, X., Huang, L., and Zhao, Y. (2023) 'The correlation between creep resistance and microstructure in AA6111 alloy strengthened by synergistic Er, Zr addition', *Materials science and engineering journal, A*, 870, 144867.
- Quainoo, G. K., and Yannacopoulos, S. (2004) 'The effect of cold work on the precipitation kinetics of AA6111 aluminum', *Journal of materials science*, 39, 6495-6502.
- Quainoo, G. K., Yannacopoulos, S., and Gupta, A. K. (2001) 'Strengthening characteristics of AA6111 aluminum', *Canadian metallurgical quarterly journal*, 40(2), 211-220.
- Raji, A. O., and Oke, S. A. (2020). 'Optimization of EDM for AA6061/10% Al₂O₃ AMMC using taguchi schemes and analytical hierarchy process for weight determination'. *Kufa Journal of Engineering*, 11(3).
- Sarkar, J., Kutty, T. R. G., Wilkinson, D. S., Embury, J. D., and Lloyd, D. J. (2004) 'Tensile properties and bendability of T4 treated AA6111 aluminum alloys', *Materials science and engineering journal, A*, 369(1-2), 258-266.
- Shurkin, P., Scamans, G., Barekar, N., Hou, L., Subroto, T., and Barbatti, C. (2023) 'Phase Composition and Microstructure of High Strength AA6xxx Aluminium Alloys with Nickel Additions', *Materials transactions journal*, 64(2), 398-405.

- Standard, A. S. T. M. (2012), E407-07 'Standard Practice for Microetching Metals and Alloys', ASTM International., West conshohocken, PA, 1-21
- Xiao, Q., Liu, H., Yi, D., Yin, D., Chen, Y., Zhang, Y., and Wang, B. (2017) 'Effect of Cu content on precipitation and age-hardening behavior in Al-Mg-Si-xCu alloys', *Journal of alloys and compounds*, 695, 1005-1013.
- Zeren, M. (2005) 'Effect of copper and silicon content on mechanical properties in Al-Cu-Si-Mg alloys', *Journal of materials processing technology*, 169(2), 292-298.
- Zhang, L., Wang, Y., Yang, X., Li, K., Ni, S., Du, Y., and Song, M. (2017) 'The texture, microstructure, and mechanical properties of 6111 aluminum alloy are subject to rolling deformation', *Materials research journal*, 20, 1360-1368.
- Zhang, S., Xiong, B., Zhang, Y., Li, X., Wang, F., Li, Z., and Liu, H. (2013) 'The Microstructural Evolution of AA6111 Aluminium Alloy during Homogenization Treatment', *In materials science forum* (Vol. 749, pp. 223-228).
- Zhen, L., Fei, W. D., Kang, S. B., and Kim, H. W. (1997) 'Precipitation behavior of Al-Mg-Si alloys with high silicon content', *Journal of materials science*, 32, 1895-1902
- Zuo, L., Ye, B., Feng, J., Zhang, H., Kong, X., and Jiang, H. (2020) 'Effect of ϵ -Al₃Ni phase on mechanical properties of Al-Si-Cu-Mg-Ni alloys at elevated temperature', *Journal of materials science and engineering: A*, 772, 138794.